ORIGINAL ARTICLE

TRIM28 inactivation in epithelial nephroblastoma is frequent and often associated with predisposing *TRIM28* germline variants

Jenny Wegert[1†], Anne Kristin Fischer[2†], Balazs Palhazi[1], Taryn D Treger[3,4,5], Cäcilia Hilgers[6], Barbara Ziegler[1], Hyunchul Jung[3], Eva Jüttner[7], Andreas Waha[8], Jörg Fuchs[9], Steven W Warmann[9], Michael C Frühwald[10], Jochen Hubertus[11], Kathy Pritchard-Jones[12], Norbert Graf[13], Sam Behjati[3,4,5], Rhoikos Furtwängler[13,14], Manfred Gessler[1,15*‡] and Christian Vokuhl[6‡]

[1] Theodor-Boveri-Institute/Biocenter, Developmental Biochemistry, University of Wuerzburg, Wuerzburg, Germany
[2] Department of Pathology, University of Cologne, Cologne, Germany
[3] Wellcome Sanger Institute, Hinxton, UK
[4] Department of Paediatrics, University of Cambridge, Cambridge, UK
[5] Cambridge University Hospitals NHS Foundation Trust, Cambridge, UK
[6] Department of Pathology, Section of Pediatric Pathology, University of Bonn, Bonn, Germany
[7] Department of Pathology, Schleswig-Holstein University Hospital, Kiel, Germany
[8] Department of Neuropathology, University of Bonn, Bonn, Germany
[9] Department of Pediatric Surgery and Pediatric Urology, University Children's Hospital Tübingen, Tübingen, Germany
[10] Swabian Children's Cancer Center, Pediatrics and Adolescent Medicine, University Hospital Augsburg, Augsburg, Germany
[11] Department of Pediatric Surgery at Marienhospital Witten, Ruhr-University Bochum, Witten, Germany
[12] UCL Great Ormond Street Institute of Child Health, University College London, London, UK
[13] Department of Paediatric Haematology and Oncology, Saarland University Hospital, Homburg, Germany
[14] Pediatric Hematology and Oncology, Inselspital Children's Hospital, University Bern, Bern, Switzerland
[15] Comprehensive Cancer Center Mainfranken, University of Wuerzburg, Wuerzburg, Germany

*Correspondence to: M Gessler, Theodor-Boveri-Institute, Developmental Biochemistry, Am Hubland, Würzburg 97074, Germany.
E-mail: gessler@biozentrum.uni-wuerzburg.de

[†]Equal contributions.
[‡]Co-senior authors.

Abstract

Wilms tumors (WTs) are histologically diverse childhood cancers with variable contributions of blastema, stroma, and epithelia. A variety of cancer genes operate in WTs, including the tripartite–motif–containing–28 gene (*TRIM28*). Case reports and small case series suggest that *TRIM28* mutations are associated with epithelial morphology and WT predisposition. Here, we systematically investigated the prevalence of *TRIM28* inactivation and predisposing mutations in a cohort of 126 WTs with >2/3 epithelial cells, spanning 20 years of biobanking in the German SIOP93–01/GPOH and SIOP2001/GPOH studies. Overall, 44.4% (56/126) cases exhibited loss of TRIM28 by immunohistochemical staining. Of these, 48 could be further analyzed molecularly, revealing *TRIM28* sequence variants in each case – either homozygous (∼2/3) or heterozygous with epigenetic silencing of the second allele (∼1/3). The majority (80%) of the mutations resulted in premature stops and frameshifts. In addition, we detected missense mutations and small deletions predicted to destabilize the protein through interference with folding of key structural elements such as the zinc–binding clusters of the RING, B–box–2, and PHD domains or the central coiled–coil region. *TRIM28*–mutant tumors otherwise lacked WT–typical *IGF2* alterations or driver events, except for rare *TP53* progression events that occurred with expected frequency. Expression profiling identified *TRIM28*–mutant tumors as a homogeneous subset of epithelial WTs that mostly present with stage I disease. There was a high prevalence of perilobar nephrogenic rests, putative precursor lesions, that carried the same biallelic *TRIM28* alterations in 7/7 cases tested. Importantly, 46% of the *TRIM28* mutations were present in blood cells or normal kidney tissue, suggesting germline events or somatic mosaicism, partly supported by family history. Given the high prevalence of predisposing variants in *TRIM28*–driven WT, we suggest that immunohistochemical testing of TRIM28 be integrated into diagnostic practice as the management of WT in predisposed children differs from that with sporadic tumors.
© 2023 The Authors. *The Journal of Pathology* published by John Wiley & Sons Ltd on behalf of The Pathological Society of Great Britain and Ireland.

Introduction

Wilms tumor (WT) or nephroblastoma is the most common renal malignancy in young children, characterized by both a diverse histological appearance and a wide range of genetic drivers. The average age at diagnosis is 1–3 years [1]. While most tumors are sporadic and unilateral, 5–8% are bilateral, or they may be familial, often associated with additional syndromic features. Multicentric tumors and a frequent association with nephrogenic rests – nodules of immature nephrogenic cells embedded in otherwise normal renal tissue – suggest the presence of WT precursors in the surrounding normal tissue that originated during kidney development [2,3]. This is consistent with the postulate that WTs represent blocked or misdirected renal development, with a step-wise progression to malignancy [4].

Cancer sequencing efforts of the past decade have identified an increasing number of genetic drivers of WTs beyond the classical WT genes *WT1*, *CTNNB1*, and *WTX*. Nearly 50 different cancer genes have been implicated, such as *SIX1*, *SIX2*, *DROSHA*, and *DICER1* [5–7]. Many of these genes are involved in normal kidney development and growth factor signaling. They orchestrate transcriptional programs, chromatin biology, miRNA processing, and genome maintenance [8]. For the most part, there is only a weak correlation between the genetic makeup and the morphology of WTs. Exceptions are the preferential association of *WT1* mutations with stromal histology or intralobar nephrogenic rests (ILNRs) and of *TP53* inactivation with an anaplastic phenotype [1].

A more recent finding is the association of *TRIM28* inactivation with epithelial-type or epithelial-predominant WT [9–11]. TRIM28 (also known as KAP1/TIF1ß) is a central transcriptional regulator protein, interacting with the family of Krüppel-associated box domain-containing zinc finger transcription factors (KRAB-ZNFs). These transcription factors mediate binding and repression at specific genomic sites, dependent on their own post-translational modifications [12,13]. TRIM28 functions as a scaffold protein, recruiting chromatin remodeling factors, and regulates induction of heterochromatin, chromatin accessibility, and transcriptional elongation. Furthermore, it is involved in transcriptional silencing of transposable elements, i.e. endogenous retroviruses (ERVs), making it essential for early vertebrate development [14,15].

TRIM28 mutations have been documented in case reports and small case series of WT [9–11,16]. Collectively, these data highlight biallelic *TRIM28* mutations in epithelial WT, with a high prevalence of predisposing variants. Key questions that remain unanswered include the degree of genotype–phenotype association, the extent of predisposition, and additional driver events in *TRIM28*-mutant tumors.

We assembled an unbiased cohort of 126 children with WT, spanning two decades of tissue banking in Germany, to systematically define the pattern of *TRIM28* mutations in epithelial-type WTs. Our work defines both the spectrum and frequency of *TRIM28* mutation and reveals a high prevalence of germline and mosaic predisposing variants. TRIM28 immunohistochemistry and mutation yielded congruent findings, thereby establishing immunohistochemistry as a practical and accessible screening tool for *TRIM28*-driven WT and, thus, for possible predispositions that influence the treatment of children with WT.

Materials and methods

Sample description

Tissues were collected and studied by consent as part of the pathology reference review and biobanking process of the SIOP93-01/GPOH and SIOP2001/GPOH studies (approved by the Ethikkommission der Ärztekammer des Saarlandes, reference numbers 23.4.93/Ls and 136/01 and 248/13). Informed consent was obtained as part of the SIOP93-01/GPOH and SIOP2001/GPOH studies. Germline genetic data were anonymized.

Immunohistochemistry/tissue microarrays (TMA)

Sections were cut at 2 μm and stained with hematoxylin and eosin (H&E) for diagnosis. Core tissue biopsies were punched from selected regions of the original paraffin blocks using a thin-wall stainless steel tube. Three 1-mm punches of tumor tissue were taken for each case. Evaluation of the TMA confirmed that the tumor tissue cores corresponded to the original block. Cores without viable tumor or artifacts were excluded.

For immunohistochemical analysis of FFPE tissue, 2-μm sections of the TMA were mounted on glass slides, and staining was carried out using a Ventana BenchMark ultra (Roche, Ludwigsburg, Germany), an automated slide staining system using an antigen retrieval (pH 8) and a Trim28/KAP1 polyclonal rabbit anti-human antibody (Abcam, Berlin, Germany, ab10484, 1:500). For visualization, UltraView DAB (Roche, Mannheim, Germany) was used following the manufacturer's protocol.

Cryosections were stained for TRIM28 with α-TRIM28 HPA064033 (Sigma, Taufkirchen, Germany) antibody and HiDef Detection HRP Polymer System (Medac, Wedel, Germany) with DAB Substrate Kit (Thermo Scientific, Dreieich, Germany).

DNA and RNA isolation

DNA from FFPE tissue was isolated using the QIAamp DNA Mini Kit (Qiagen, Hilden, Germany) as follows: sections were deparaffinized and rehydrated, and tissue was scraped from slides and digested in ATL buffer with proteinase K overnight at 56 °C. To ensure an efficient lysis, AL buffer was added for 1 h at 90 °C. The remaining steps were performed following the manufacturer's protocol. DNA was quantified via the QuantiFluor ONE dsDNA System (Promega, Walldorf, Germany).

DNA and RNA were isolated from fresh frozen tumor material and normal kidney tissue using the AllPrep DNA/RNA Mini kit (Qiagen). Genomic DNA of white blood cells was isolated as described previously [17].

PCR and Sanger sequencing

All *TRIM28* exons and flanking regions were amplified by PCR and subjected to Sanger sequencing. Reverse transcription of RNA from frozen samples used random hexamer primers and Revert Aid Reverse Transcriptase (Thermo Fisher Scientific, Waltham, MA, USA). All primer sequences are given in supplementary material, Table S1.

TRIM28 methylation analysis

Genomic DNA (0.25 µg) was treated with sodium bisulfite using the EpiTect Bisulfite kit (Qiagen) following the manufacturer's recommendations. A pyrosequencing assay was established targeting 19 CpG dinucleotides in a CpG island in the promoter of the *TRIM28* gene (chr19: 59,055,551–59,055,948 (hg19), supplementary material, Table S1. PCR was performed using the Pyromark PCR Kit (Qiagen) with 15 min at 95 °C, followed by 50 cycles of 94, 56, and 72 °C, 30 s each, and finally 72 °C for 10 min. Single-stranded DNA templates were purified using streptavidin-sepharose high-performance beads (GE Healthcare, Solingen, Germany) using the PSQ Vacuum Prep Tool and Worktable (Biotage, Düsseldorf, Germany). Pyrosequencing was performed using PyroMark® Gold Reagents (Qiagen) on the Pyromark Q24 instrument (Biotage), following the manufacturer's instructions. Pyrogram outputs were analyzed using the PyroMark CpG quantification software (Qiagen).

The overall methylation level was determined by taking the mean of the arithmetic point of the pyrosequencing methylation data from all 19 CpG positions. Normal kidney tissue samples and wildtype tumors showed only traces of methylation (~4%) and were scored as not methylated. Tumor samples were scored negative if they did not exceed the eightfold standard deviation (15.4%) of unmethylated wildtype and normal tissue. Samples with a higher average of methylation were classified as methylated.

IGF2 methylation–specific multiplex ligation-dependent probe amplification (MS-MLPA)

Methylation status of the imprinting centers at chromosome 11p15 was determined using the MS-MLPA Probemix ME030 BWS/RSS (MRC Holland, Amsterdam, Netherlands) following the manufacturer's instructions. PCR products were analyzed on an ABI 3730 DNA Analyzer (Applied Biosystems, Weiterstadt, Germany) and interpreted using Coffalyser.Net (https://www.mrcholland.com/technology/software/coffalyser-net, last accessed 17 August 2023).

Protein analyses

TRIM28 mutations were engineered into the pCS2P-HA-TRIM28 expression vector and verified by Sanger sequencing. *TRIM28*-knockout HEK293 cells [18] were transiently transfected using polyethylenimine and treated with cycloheximide (Roth, Karlsruhe, Germany, 100 µg/ml) in the absence or presence of the proteasome inhibitor MG132 (Sigma-Aldrich, Taufkirchen, Germany, 10 µM). SDS lysates were subsequently analyzed by western blotting as described using a polyclonal HA-tag antibody (Abcam ab9110) [19].

RNA sequencing and analysis

RNA libraries were sequenced using the Illumina HiSeq 4000 platform (Illumina Inc., Cambridge, UK). Reads were aligned using STAR, and read counts of genes were obtained using HTSeq [20,21]. Data were processed in R using Edge R, normalized using the trimmed mean of M-values method, and converted to log-counts per million (CPM) values [22]. Differential expression analysis was performed using Limma and Glimma [23,24]. Telescope with the default parameters was used to measure mRNA expression level of ERVs [25]. Differentially expressed ERVs were determined based on normalized read counts by CPM. Statistical significance was assessed using the Mann–Whitney test.

Results

Overview of cohort

To provide an unbiased view of the *TRIM28* status in epithelial WTs, we assembled a cohort of all WT diagnosed in Germany between 2000 and 2020 that contained at least 2/3 epithelial cells. In total, 153 out of 1952 cases (7.8%) from the SIOP93-01/GPOH and SIOP2001/GPOH pediatric renal tumor studies were diagnosed as epithelial-type WT, i.e. containing less than 67% regression and >2/3 of epithelial cells in viable tumor after preoperative chemotherapy, as validated by one of two reference pathologists. These were supplemented with epithelial WT harboring anaplasia, a morphological feature associated with poor prognosis that overrides classification as epithelial WT in clinical guidelines. For 126 tumors (120 without anaplasia, six with anaplasia) formalin-fixed and/or fresh frozen material was available for further studies. Seven of these cases had been reported earlier [9].

TRIM28 immunohistochemistry

Tissue microarrays containing triplicates core biopsies from each of 126 tumors, as well as control tissues, showed complete loss of TRIM28 staining in 53 cases (42%), while three cases exhibited at least partial negativity in a mosaic-like pattern (WT5, WT8, WT17) (Figure 1). Five of these 56 tumors with TRIM28 loss displayed anaplasia – enlarged hyperchromatic nuclei and atypical
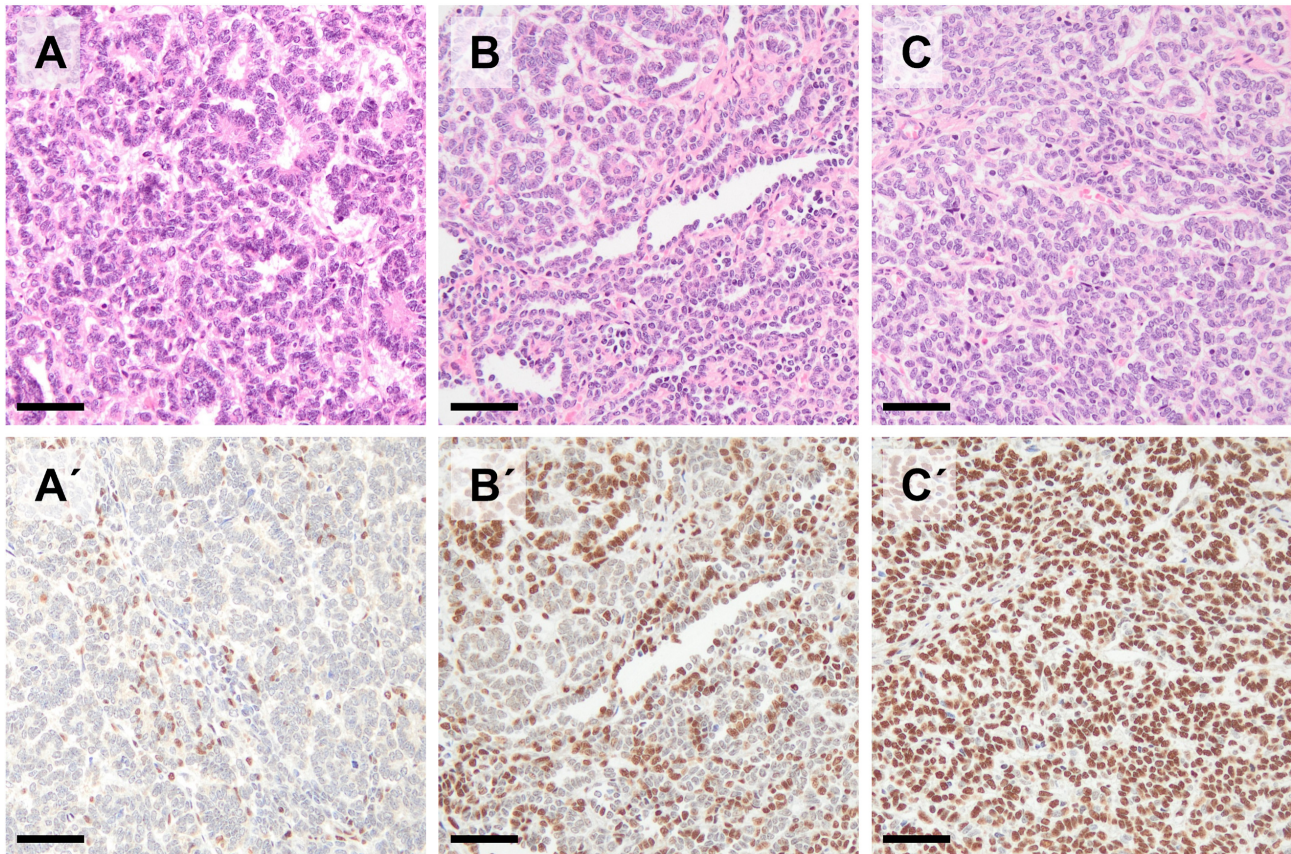
Figure 1. Immunohistochemical TRIM28 staining and morphology. Tumor sections were stained with hematoxylin and eosin (upper panels) and TRIM28 antibody (lower panels). WT19 with a frameshift S49Pfs*36 mutation showed loss of TRIM28 expression (A, A'). WT05 with a C209Y missense mutation showed mosaic positivity for TRIM28 (B, B'). WT71 with wildtype *TRIM28* retained TRIM28 expression (C, C'). Scale bars, 20 μm.

mitotic figures – in addition to epithelial-predominant histology (WT52-WT56). The remaining 70/126 cases stained positive for TRIM28 (supplementary material, Table S2).

A subset of TRIM28-negative WTs ($n = 49/53$) could be evaluated for the presence of nephrogenic rests (Table 2 and supplementary material, Table S2). We detected perilobar nephrogenic rests (PLNRs) in 30/49 (61%) tumors but no cases containing ILNRs. In seven PLNRs, we were able to assess TRIM28 status to demonstrate loss of staining. TRIM28-positive cases (66/70 assessable cases), on the other hand, harbored nephrogenic rests less frequently (42%) and exhibited greater diversity (19 perilobar, five intralobar, three both types, and one not specified).

TRIM28 sequence alterations

To search for underlying mutations in the 56 TRIM28-negative cases (complete and mosaic), all *TRIM28* exons were sequenced in DNA from FFPE tissue (15 cases), frozen tumor (seven cases), or both (34 cases). In 21 cases, whole-genome or whole-exome sequencing data were available for tumor and control DNA to determine *TRIM28* status. Sufficient tumor content had been ascertained by H&E staining of adjacent sections.

We found truncating mutations, nonsense or frameshift indels, in 30 tumors (Table 1 and supplementary material, Table S2). In eight tumors, mutations affected splice sites, resulting in exon skipping with consecutive frameshifts as verified by RT-PCR analysis. In addition, there were nine cases with in-frame deletions, missense, and readthrough mutations. The latter were predicted to lead to nonstop-mediated mRNA degradation as there is no other in-frame stop codon in the 3'-UTR. One tumor (WT43) harbored a larger deletion spanning exons 7 to 9. In eight cases, only low-quality DNA was obtained from FFPE material, and PCR amplification failed for several exons, precluding mutation testing (WT44-51). Overall, we were able to screen 48/56 TRIM28 negative tumors and found sequence alterations of the *TRIM28* gene in every case.

Specificity of *TRIM28* mutations

For 32 of the epithelial-type WTs that stained positive for TRIM28, whole-genome sequencing (WGS) data were available as part of a larger cohort of 410 WT cases (T.T., personal communication). These tumors did not harbor *TRIM28* mutations, ruling out the presence of nonfunctional mutant proteins that might still be detected by immunohistochemistry. Instead, these tumors carried mutations in other known WT drivers, such as *MLLT1*, *CTNNB1*, and *WT1* (T.T., personal communication).

Table 1. Characteristics of TRIM28-negative WT.

ID	TRIM28 AA change (NP_005753)	Tumor	Methylation tumor	Germline or mosaic status	TP53 status	Multifocal/ bilateral	Histology
WT1	C65R	het	nd	wt (K)		No	E
WT2	C117G	het	+	wt (B)	wt	No	E
WT3	C117F	hom		het (K)	neg	No	E
WT4	C120Y	hom		wt (B)		No	E
WT5	C209Y	het	+	wt (K)	neg	No	E
WT6	C224Y	hom		wt (K)	neg	No	E
WT7	H240N	het	−	het (B, K)	neg	n.i.	E
	K304delK	het		wt (B, K)			
WT8	R290P	het	+	wt (K)	wt	No	E
WT9	*836W	hom		wt (B)	wt	MF	E
WT10-T1	E179fs*1	het	+	wt (B)	neg	MF	E
WT10-T2	Q331*	het	+	wt (B)	wt	MF	E
WT11	R230*	hom		wt (B)	wt	No	E
WT12[1]	Q283*	hom		het (B)	neg	No	E
WT13[1]	Q283*	hom		het (B)	wt	BL	E/PLNR
WT14[2]	Q339*	hom		het (B, K)	neg	MF, BL	E/E
WT15	R487*	het	+	wt (B, K)	neg	No	E
WT16	R487*	het	+	wt (B, K)	neg, R342delR	No	E
WT17	Q502*	het	nd	wt (K)	neg	No	E
WT18	Q701*	het	+	wt (B, K)	wt	No	E
WT19	S49Pfs*36	hom		wt (B, K)	neg	No	E
WT20	L59Wfs*34	hom		het (B, K)	wt	No	E
WT21	R71Sfs*23	het	+	wt (B, K)	wt	No	E
WT22	E77fs*13	hom		het (B, K)	wt	BL	E#/T
WT23	C174Rfs*4	hom		het (K)	neg	BL	E#/PLNR#
WT24	C174fs*1	hom		het (B)	wt	No	E
WT25	S138G & S140Hfs*12	hom		n.d.	neg	No	E
WT26	H190Qfs*25	het	+	wt (B)	neg	No	E
WT27	C221fs*25	hom		het (K^m)	wt	No	E
WT28	N307Cfs*5	hom		n.d.		No	E
WT29	E322Gfs*34	het	+	wt (K)	neg	No	E
WT30	L362Wfs*6	hom		het (B, K)	wt	MF	E
WT31	M389Rfs*2	het	+	wt (K)	wt	No	E
WT32	G406Afs*27	hom		wt (B, K)	neg	n.i.	E#
WT33	S512Ifs*164	hom		het (B)		BL	E/E
WT34	A560Lfs*115	het, monoallelic expr.	−	het (B, K)	neg	No	E
WT35	P572Rfs*16	hom		het (B)	wt	No	E#
WT36	Splice Ex3 + 2	hom		het (B)	neg	BL	E/PLNR
WT37	Splice Ex4 + 1	hom		wt (B)	neg	No	E
WT38	Splice Ex10 + 5	hom		n.d.		n.i.	E
WT39	Splice Ex11 + 2	hom		het (B)	neg	No	E#
WT40	Splice Ex4	het	−	wt (B)		No	E
	Splice Ex13 + 1	het		wt (B)			
WT41	Splice Ex14 + 2	het	+	wt (B)	neg	No	E
WT42	Splice In14	hom		het (K)	neg	BL	E/E
WT43	del Ex7-Ex9 (Q342-P426)	het	+	het (K)	wt	No	E
WT44	insuff. DNA					No	E
WT45	insuff. DNA				neg	No	E
WT46	insuff. DNA				neg	No	E
WT47	insuff. DNA				neg	n.i.	E
WT48	insuff. DNA				neg	n.i.	E
WT49	insuff. DNA					n.i.	E
WT50	insuff. DNA					MF	E
WT51	insuff. DNA				neg	MF	E
WT52	Q339*	hom		het (B)	wt	No	FA (E)
WT53	P118Afs*59	het	+	wt (B, K)	pos	No	FA (E)
WT54	V207fs*10	hom		wt (K)	pos, R248Q	No	DA (E)
WT55	A544Pfs*132	hom		het (K^m)	pos, R175H	No	DA (E)
WT56	Splice Ex6 + 1	hom		wt (B, K)	N131delN	n.i.	DA (E)
WT127	R487*	hom		wt (B)	deletion	n.i.	DA (B)

(Continues)

Table 1. Continued

ID	TRIM28 AA change (NP_005753)	Tumor	Methylation tumor	Germline or mosaic status	TP53 status	Multifocal/ bilateral	Histology
WT128	Splice Ex5 + 1	hom		wt (B)	wt	No	R
WT129	*836W hom	hom		het (B)	wt	No	R
WT130	C91W	hom		het (K)	wt	No	T
WT131 [2]	R524fs*155	hom		het (K)	wt	No	T
WT132	R629_C631delRVC	hom		het (B)	wt	No	PLNR
WT133	S50Rfs*36	hom		wt (B)	neg	No	PLNR#
WT134	P753Afs*20	het	n.d.	n.d.	neg	No	PLNR#

[1], monozygotic twins.
[2], familial WT.

het, heterozygous; hom, homozygous; −, unmethylated; +, hypermethylated; B, blood; K, kidney; m, mosaic; TP53 status: neg, negative by p53 IHC; pos, positive by p53 IHC (presumed stabilizing mutation); wt, wildtype TP53 (according to sequencing), with known mutations indicated; MF, multifocal; BL, bilateral; E, epithelial; B, blastemal; R, regressive; T, triphasic; FA, focal anaplasia; DA, diffuse anaplasia; PLNR, perilobar nephrogenic rest; # primary surgery before chemotherapy; n.d., not analyzed; n.i., no information.

In contrast, the 21 TRIM28-negative tumors that had been analyzed by WGS did not carry alterations in any of these WT-typical drivers. The only exceptions were *TP53* mutations as a presumed progression event found at a low frequency in both the TRIM28-positive and TRIM28-negative subsets. These tumors often exhibited diffuse anaplasia.

To evaluate the specificity of *TRIM28* mutations for epithelial differentiation in WTs, we screened the remainder of the whole genome cohort (n = 378) for genetic changes in *TRIM28*. We detected *TRIM28* mutations in eight additional cases, five WTs and three cases of nephroblastomatosis. These cases had not met the diagnostic criteria of epithelial-type Wilms due to regression or the presence of higher amounts of nonepithelial cells (Table 1 and supplementary material, Table S2). Again, four out of five WTs had concomitant PLNRs. In summary, these findings indicate that TRIM28 variants mostly occur in epithelial WT.

Biallelic inactivation of *TRIM28*

Most *TRIM28* mutations were homozygous in tumor tissue. There was copy number neutral loss of the wildtype allele in 34/56 sequenced cases, while two cases showed somatic deletion of the wildtype allele (Table 1 and supplementary material, Table S2). Two cases harbored two mutations each: WT7 with germline

Table 2. Clinical characteristics of WT according to histology and *TRIM28* status.

		Epithelial type (>65%) *TRIM28* mutant	Nonepithelial type *TRIM28* mutant	Epithelial type (>65%) *TRIM28* wildtype
Total	N =	56	8	70
Sex	F	30	5	44
	M	26	3	26
Age at diagnosis	Median and range (months)	10.8 (3.6–163.3)	67.3 (13.4–152.6)	33.0 (1.2–200.1)
Stage	I	44	5 (+3 NBL)	44
	II	1	0	13
	III	1	0	5
	IV	3	0	3
	V	7	0	5
Nephrogenic rests	PLNR	30	4 (+3 NBL)	19
	ILNR	0	0	5
	Both	0	0	3
	Not specified	0	0	1
	None	19	1	38
	Not reported	7	0	4
IGF2 methylation	wt	39	7	10
	LOI/LOH	2	0	14
	n.d.	15	0	46
TP53 status	pos/mut	5	1	4
	neg/wt	42	7	57
	n.d.	9	0	9
Outcome	Second event	5	1	9
	Death	3	0	3
Median follow-up	(months)	41.9	50.4	60

ILNR, intralobar nephrogenic rest; LOH, loss of heterozygosity; LOI loss of imprinting; mut, mutation; NBL, nephroblastomatosis; n.d., not analyzed; neg, negative; PLNR, perilobar nephrogenic rests; pos, positive; wt, wildtype.

H240N and somatic K304Kdel; WT40 with two independent splice site variants in tumor material, both absent from normal control tissue. RNA analysis confirmed that both alleles were affected, indicating a compound heterozygous state.

We did not find a second DNA sequence alteration in 18/56 *TRIM28*-mutant tumors. For 15 of these, expression analysis was possible, which revealed that the vast majority of transcripts were derived from the mutant allele with apparent silencing of the remaining wildtype allele. Methylation analysis of a CpG island in the *TRIM28* promoter region by pyrosequencing then revealed hypermethylation in 14/15 tumors with monoallelic expression, whereas both compound heterozygous tumors with biallelic expression and 6/6 *TRIM28*-wildtype tumors showed no evidence of DNA methylation in this region. In a single case (WT34), a heterozygous frameshift mutation was seen, but the tumor exhibited exclusive expression of the mutant allele without somatic hypermethylation. The underlying mechanism of inactivation of the wildtype allele is unclear. It may involve upstream alterations in control regions that would not be detected by our sequencing methods. In three cases, DNA extracted from FFPE material was not suitable for pyrosequencing. Allelic silencing is thus a common means to complete inactivation of *TRIM28* in heterozygous situations.

In total, a molecular cause for *TRIM28* inactivation was identified in 56 WT cases: 13 amino acid changes (nine missense, two in-frame deletions, and two readthrough) and 46 null mutations (11 nonsense, 24 frameshift, 10 splice site, and one multi-exon deletion) were detected (Figure 2).

## Germline mutations are frequent

TRIM28 mutations have been shown to be present in the germline in 27 patients (summarized in 26). However,

the frequency of genetic predisposition in an unselected cohort and the distinction between germline and somatic mosaicism remain unclear. For 52/56 *TRIM28*-mutant cases, blood samples and/or adjacent normal kidney tissues were available for study. In 24/56 cases (46%) we found mutations in blood (*n* = 16) or in normal kidney tissue (*n* = 8) where blood was unavailable. In four patients, two of them monozygotic twins, there was clear evidence of heritability given a family history of WT (Table 1). Of note, in the seven cases in which we were able to analyze PLNRs adjacent to *TRIM28*-mutant WTs (see preceding discussion), the DNA from nontumorous PLNR tissue showed the same *TRIM28* mutation (supplementary material, Table S2).

Missense mutations destabilize TRIM28

Previous reports documented truncating mutations in *TRIM28* as the predominant alteration in the gene. We now identified 11 missense mutations and two in-frame deletions. We placed these variants onto the known 3D structure of TRIM28, which suggested a common mechanism for disruption of TRIM28 function, as all mutations were located in critical regions of the protein [26–28].

In the RING domain (C3HC4), cysteines 65/91 and 117/120 are part of two essential Zn^{2+} coordinating clusters [28]. The C65R, C91W, C117F/G, and C120Y mutations are expected to prevent the formation of the zinc finger structure and, thus, to destabilize the protein [29]. Similarly, B-box 2 is a RING-like motif (CHC4H2-type) with dual cross-braced Zn^{2+} coordination, extending from cysteine 209 to histidine 240 [28]. The C209Y, C224Y, and H240N mutations may thus likewise impair B-box 2 folding and destabilize the mutant protein [26,27]. The more distal deletion R629_C631delRVC in WT132 affects the PHD domain, where cysteine 631 is part of a zinc binding cluster that is essential for autosumoylation and target
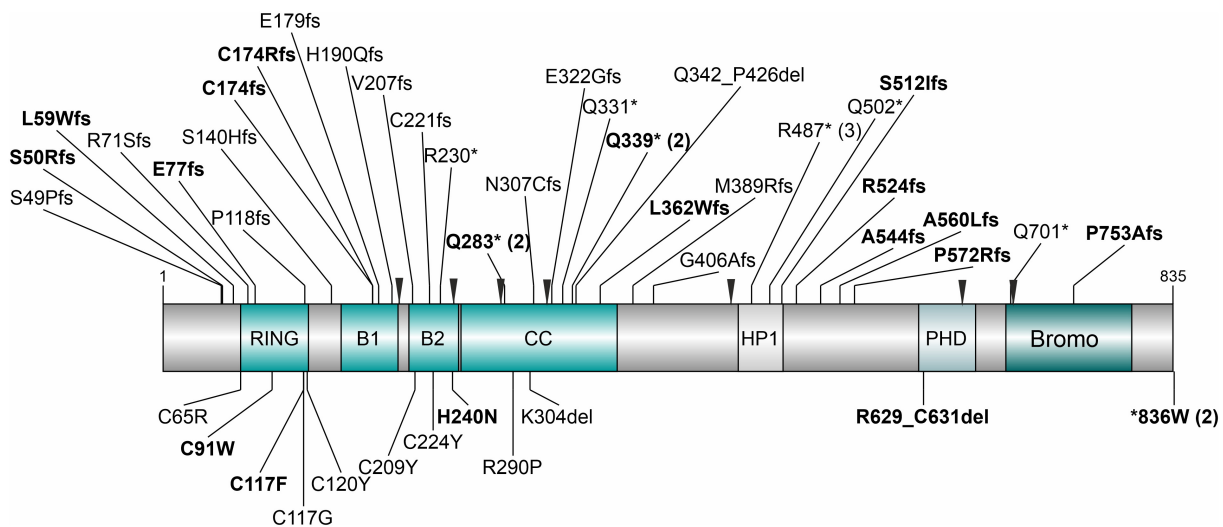
Figure 2. Distribution of mutations across TRIM28 protein. Protein domains are indicated by boxes. Null mutations (nonsense and frameshift) are shown in upper panel, while missense, small in-frame deletions, and read-through mutations are indicated in lower panel. Splice site mutations are highlighted by arrowheads. Mutations present in the germline are shown in bold. The NP_005753.1 reference sequence was used for amino acid numbering.

gene repression as shown before [30]. Finally, the K304del mutation in WT7 disrupts heptad periodicity of a four-helix bundle in the center of the coiled coil domain that interacts with the KRAB domain of DNA-binding zinc finger transcription factors to mediate transcriptional silencing. A similar K304E mutation has been shown to decrease the affinity of TRIM28 for the ZNF932 KRAB domain by three orders of magnitude, which would abolish its gene-silencing capacity [26].

We demonstrated the proposed missense mutation-induced destabilization of TRIM28 directly by expressing wildtype and mutant TRIM28 proteins in HEK293T cells lacking endogenous TRIM28 [18]. While all proteins were expressed, the half-life of the mutants was shortened, as evidenced by a decrease in protein levels upon translation arrest by cycloheximide exposure (Figure 3). Additional blockade of the proteasome again stabilized the mutant proteins. As this effect was seen with different missense mutations, we expect this to be a common mechanism applicable to most missense mutants. Nevertheless, partial protein stability together with incomplete silencing of the remaining wildtype allele may be the reason for the mosaic TRIM28 expression seen in three cases (WT5, WT8, WT17; see Table 1).

Expression profiling

While TRIM28 IHC and mutation status clearly define two subgroups of epithelial WTs, there is no morphological correlate of this difference. RNA sequencing (RNA-seq) data were available on 23 TRIM28-wildtype and 21 TRIM28-mutant WT (T.T. *et al*, unpublished) to elucidate differences between these two groups. Tumors with an additional TP53 mutation were excluded from this analysis. 135 genes were differentially expressed with a minimum log2-fold change of 1, with 123 of these upregulated in mutant tumors (supplementary material, Table S3). Unsupervised clustering clearly separated mutant from wildtype tumors, regardless of whether they had null or missense mutations (Figure 4). Only one of the two tumors with a stop-loss mutation (WT9) was

grouped with wildtype samples, while the second tumor (WT129) clustered with the other TRIM28-mutant cases. The differentially expressed genes do not point to specific cellular functions being affected. Among the genes upregulated in TRIM28-mutant tumors there was a much higher fraction of lncRNAs and pseudogenes (32% and 16%, $N = 123$), compared to wildtype cases (17% and 0%, $N = 12$). This is in line with TRIM28 being involved in repression of transposable elements. Indeed, expression analysis of transposable elements confirmed the clear separation of epithelial WTs with strongly enhanced expression of the HERVI, HERV3, PABLB, and HERVFC2 families, among others, upon TRIM28 mutation (Table 3).

IGF2 methylation

IGF2 overexpression, due to imprinting defects on chromosome 11p15, is a common event in Wilms tumorigenesis. We analyzed the corresponding IC1 imprinting center in TRIM28-mutant and -wildtype tumors by methylation-specific MLPA. A normal methylation status, with one methylated and one unmethylated allele, was detected in 45/48 (94%) of mutant cases (Table 2). The converse was true in TRIM28-wildtype cases, where 63% (15/24) showed two unmethylated alleles due to loss of heterozygosity (LOH) or loss of imprinting (LOI), comparable to other WT cohorts. Thus, TRIM28-mutant tumors are not dependent on elevated expression of mitogenic IGF2 as seen in most WTs.

Clinical correlates

There is a striking difference in the age distribution of the TRIM28-mutant versus TRIM28-wildtype cohorts (Table 2). The median age at diagnosis of TRIM28-wildtype epithelial tumors was 33.0 (range 1.2–200.1) months, while TRIM28-mutant epithelial tumors were diagnosed at a median age of 10.8 (range 3.6–163.3) months. Comparison of cases with presumed germline versus somatic TRIM28 mutations revealed a further distinction, with median ages of 8 versus 11 months, respectively. On the other hand, the small subgroup of TRIM28-mutant
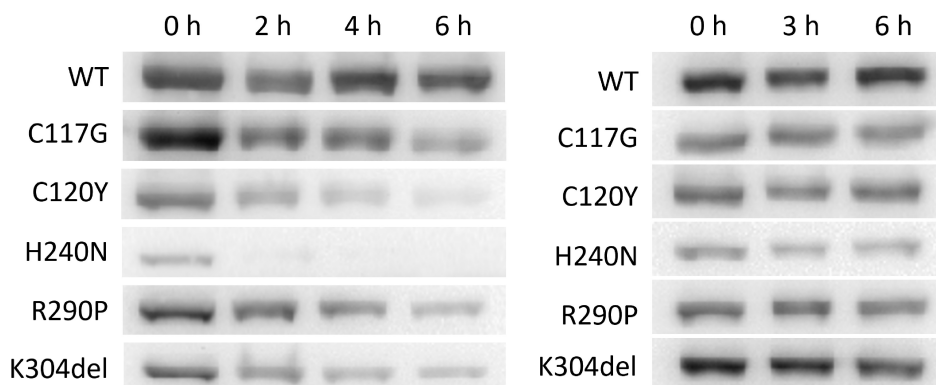
Figure 3. Stability of mutant TRIM28 protein. TRIM28-knockout HEK293 cells were transiently transfected with expression vectors for wildtype or mutant TRIM28 as indicated on left. TRIM28 western blots of parallel cultures treated with cycloheximide (left) or cycloheximide plus MG132 (right) for the times indicated.
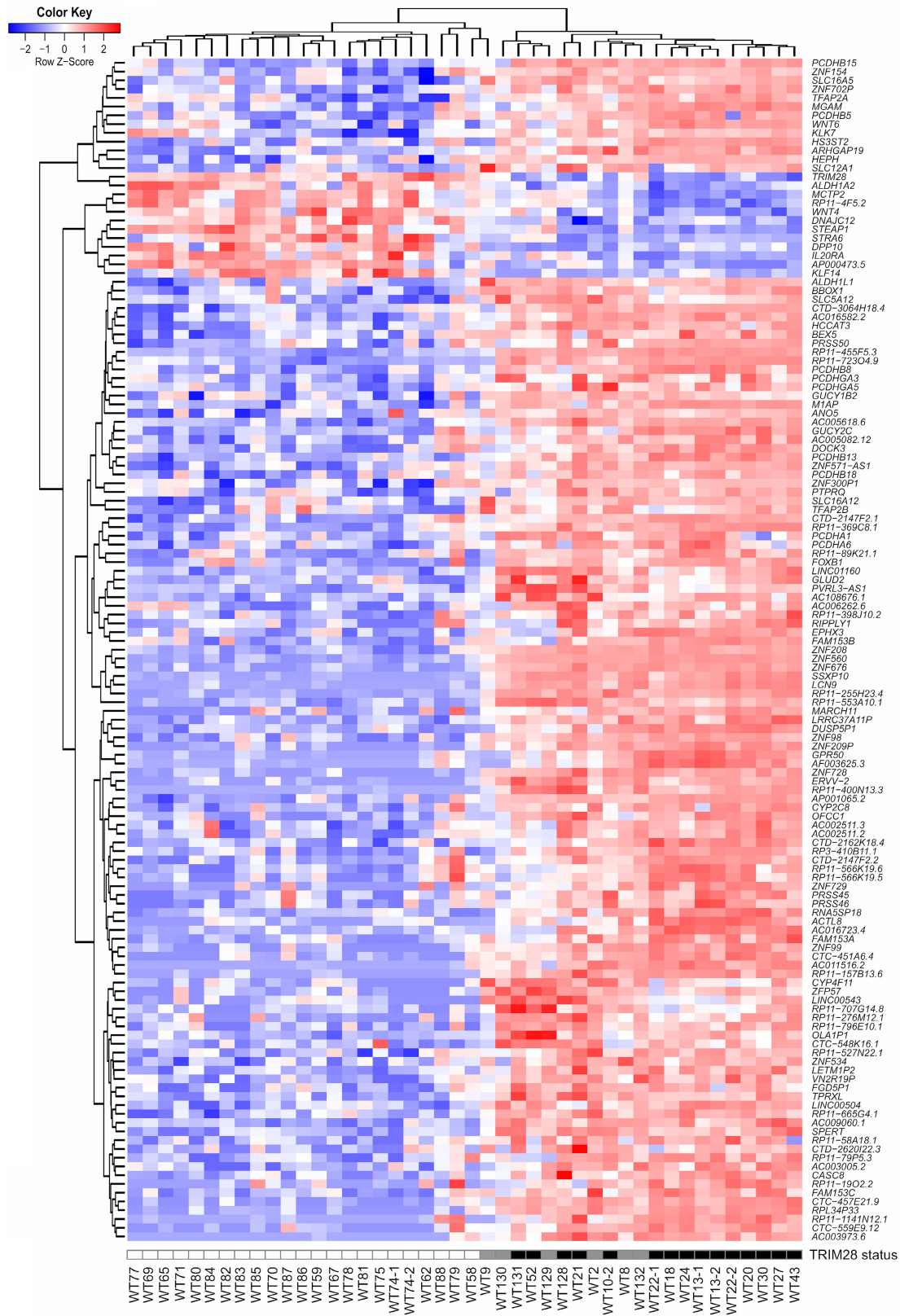
Figure 4. RNA expression profiling: unsupervised clustering of differentially expressed genes in *TRIM28*-wildtype versus *TRIM28*-mutant tumors with a log2-fold-change ≥1. *TRIM28* status: white = wildtype, gray = missense or readthrough mutation, black = null mutation.

tumors classified as regressive, triphasic, or blastemal with diffuse anaplasia was diagnosed even later, at the age of 67.3 (range 13.4–152.6) months.

While gender distribution was almost equal in TRIM28-mutant cases (35 female, 29 male), there was a nonsignificant trend toward a gender bias in

Table 3. Average expression levels of ERV families of transposable elements in *TRIM28*-mutant and wildtype WTs.

ERV family	*TRIM28*-mutant CPM_Average	*TRIM28*-wildtype CPM_Average	Fold-change	*P* value
HERVI	220.04	16.55	13.29	1.28E-08
HERV3	281.99	54.10	5.21	1.47E-08
PABLB	57.68	4.18	13.81	1.47E-08
HERVFC2	0.20	0.05	4.15	9.66E-07
HML1	43.56	17.43	2.50	1.16E-06
HML6	111.24	74.19	1.50	1.30E-05
HML4	81.04	52.63	1.54	3.58E-05
HERVW	29.40	20.05	1.47	6.43E-04
HERVE	72.11	50.90	1.42	8.89E-04
HERVK14C	7.09	4.78	1.49	1.66E-03
HERVH	252.61	170.03	1.49	3.21E-03
HERVFRD	16.03	10.86	1.48	4.25E-03
HML2	73.21	48.51	1.51	9.39E-03
HML3	99.60	78.28	1.27	1.13E-02
HERVH48	17.26	12.91	1.34	2.42E-02
HML5	42.01	34.41	1.22	4.31E-02

Expression levels are count per million average values of 21 (mutant) and 23 (wildtype) tumors.

TRIM28-wildtype epithelial WT, with 44 female and 26 male patients. Most TRIM28-mutant cases were stage I, with an excellent prognosis. Of 24 patients with a mosaic or germline *TRIM28* predisposition, eight had bilateral or multifocal disease, while only two multifocal tumors occurred in the absence of a predisposing *TRIM28* mutation. Since only blood was available in some of these cases, mosaic mutations in the surrounding kidney cannot always be excluded.

Discussion

We have defined the spectrum of *TRIM28* alterations, corroborating the association between *TRIM28* variants and epithelial morphology. Of note, we were able to demonstrate complete concordance of immunohistochemical nuclear loss of TRIM28 and molecular *TRIM28* alterations. This suggests that immunohistochemistry may lend itself to being a screening tool for *TRIM28* mutations. In almost half of the cases, one mutation was cancer predisposing, i.e. present in the germline or in normal kidney. Loss of TRIM28 staining in WTs can therefore be used to identify children with a genetic WT predisposition, for whom mutation screening and genetic counseling may be advised.

While previous work established an association of TRIM28 mutation with epithelial WT [9–11,16], our work represents the first systematic effort in a large cohort of WT. Based on national registration data, we are likely to have captured the vast majority of WT cases in Germany over two decades. As such, our work represents a largely unbiased analysis of *TRIM28* mutation in epithelial WT. Our findings are broadly applicable to children with WT who received neoadjuvant chemotherapy prior to nephrectomy and may be conceivably applicable to treatment-naïve tumors in the same way.

Most tumors with TRIM28 loss harbored biallelic inactivation of *TRIM28*, consistent with a recessive pattern of mutation. In addition to truncating mutations, which account for 44/46 cases from prior reports [31], we identify missense and in-frame indels of *TRIM28* predicted to disrupt protein stability. In particular, mutations of cysteine or histidine residues in critical zinc coordinating clusters of the RING, B2, and PHD domains appear to affect protein folding and stability. Other variants that lie in the same domains as our mutations were previously shown to impair protein function [26–28,30]. It would therefore seem likely that the nontruncating mutations we found alter protein stability as well as function.

TRIM28-mutant tumors were associated with a high proportion of PLNRs but not ILNRs. These are residual embryonic renal cell clusters composed of blastemal or immature epithelial cells, considered to be possible precursor lesions for WTs [32]. Interestingly, we found that PLNRs carried the same *TRIM28* changes as associated adjacent tumors, suggesting that the mutation is an early, likely tumor-initiating event.

TRIM28-mutant epithelial WTs delineate a subset of children with WT with specific clinical characteristics, such as young age, an elevated risk of multifocal and bilateral tumors, and an increased risk of germline predisposition. Although these tumors have an excellent prognosis overall [33,34], there are nuances in the management of children with WT when a predisposition is identified. This may include efforts for nephron-sparing surgery to preserve functional kidney tissue in the case of metachronous tumors, adaptation of treatment recommendations and an extended follow-up [35]. It is therefore important to identify children with *TRIM28*-mutant WT as, according to our findings, almost half of these individuals may harbor a predisposing mutation. Accordingly, we would recommend that TRIM28 staining be incorporated into the routine diagnostic work-up of WT. This should include all tumors in order not to miss cases where epithelial features are masked by classification as regressive or anaplastic.

Acknowledgements

Author contributions statement

The concept of the study was developed by MG, JW and CV. Essential materials and data sets were provided by NG, RF, SWW, JF, JH, MCF and EJ. Data were generated and analyzed by JW, BP, CH, BZ, AW and AKF. WGS data analysis and RNA-seq visualization were performed by TDT, SB, JW, MG, HJ and KP-J. The study was supervised by JW, CV and MG. The original draft was written by MG, JW, CV and AKF. All authors contributed to revisions of the manuscript and approved the final version.

Data availability statement

Coordinates of all mutations are given in supplementary material, Table S2; genome sequencing data will be part of a subsequent publication (Treger *et al*).

References

1. Spreafico F, Fernandez CV, Brok J, *et al*. Wilms tumour. *Nat Rev Dis Primers* 2021; **7**: 75.
2. Coorens THH, Treger TD, Al-Saadi R, *et al*. Embryonal precursors of Wilms tumor. *Science* 2019; **366**: 1247–1251.
3. Fialkowski E, Sudour-Bonnange H, Vujanic GM, *et al*. The varied spectrum of nephroblastomatosis, nephrogenic rests, and Wilms tumors: review of current definitions and challenges of the field. *Pediatr Blood Cancer* 2022: e30162.
4. Behjati S, Gilbertson RJ, Pfister SM. Maturation block in childhood cancer. *Cancer Discov* 2021; **11**: 542–544.
5. Gadd S, Huff V, Walz AL, *et al*. A Children's oncology group and TARGET initiative exploring the genetic landscape of Wilms tumor. *Nat Genet* 2017; **49**: 1487–1494.
6. Walz AL, Ooms A, Gadd S, *et al*. Recurrent DGCR8, DROSHA, and SIX homeodomain mutations in favorable histology Wilms tumors. *Cancer Cell* 2015; **27**: 286–297.
7. Wegert J, Ishaque N, Vardapour R, *et al*. Mutations in the SIX1/2 pathway and the DROSHA/DGCR8 miRNA microprocessor complex underlie high-risk blastemal type Wilms tumors. *Cancer Cell* 2015; **27**: 298–311.
8. Walz AL, Maschietto M, Crompton B, *et al*. Tumor biology, biomarkers, and liquid biopsy in pediatric renal tumors. *Pediatr Blood Cancer* 2023; **70**: e30130.
9. Diets IJ, Hoyer J, Ekici AB, *et al*. TRIM28 haploinsufficiency predisposes to Wilms tumor. *Int J Cancer* 2019; **145**: 941–951.
10. Halliday BJ, Fukuzawa R, Markie DM, *et al*. Germline mutations and somatic inactivation of TRIM28 in Wilms tumour. *PLoS Genet* 2018; **14**: e1007399.
11. Armstrong AE, Gadd S, Huff V, *et al*. A unique subset of low-risk Wilms tumors is characterized by loss of function of TRIM28 (KAP1), a gene critical in early renal development: a children's oncology group study. *PLoS One* 2018; **13**: e0208936.
12. Czerwińska P, Mazurek S, Wiznerowicz M. The complexity of TRIM28 contribution to cancer. *J Biomed Sci* 2017; **24**: 63.
13. Iyengar S, Farnham PJ. KAP1 protein: an enigmatic master regulator of the genome. *J Biol Chem* 2011; **286**: 26267–26276.
14. Rowe HM, Jakobsson J, Mesnard D, *et al*. KAP1 controls endogenous retroviruses in embryonic stem cells. *Nature* 2010; **463**: 237–240.
15. Cammas F, Mark M, Dolle P, *et al*. Mice lacking the transcriptional corepressor TIF1beta are defective in early postimplantation development. *Development* 2000; **127**: 2955–2963.
16. Mahamdallie S, Yost S, Poyastro-Pearson E, *et al*. Identification of new Wilms tumour predisposition genes: an exome sequencing study. *Lancet Child Adolesc Health* 2019; **3**: 322–331.
17. Wittmann S, Zirn B, Alkassar M, *et al*. Loss of 11q and 16q in Wilms tumors is associated with anaplasia, tumor recurrence, and poor prognosis. *Genes Chromosomes Cancer* 2007; **46**: 163–170.
18. Tie CH, Fernandes L, Conde L, *et al*. KAP1 regulates endogenous retroviruses in adult human cells and contributes to innate immune control. *EMBO Rep* 2018; **19**: e45000.
19. Salat D, Winkler A, Urlaub H, *et al*. Hey bHLH proteins interact with a FBXO45 containing SCF ubiquitin ligase complex and induce its translocation into the nucleus. *PLoS One* 2015; **10**: e0130288.
20. Anders S, Pyl PT, Huber W. HTSeq-a python framework to work with high-throughput sequencing data. *Bioinformatics* 2015; **31**: 166–169.
21. Dobin A, Davis CA, Schlesinger F, *et al*. STAR: ultrafast universal RNA-seq aligner. *Bioinformatics* 2013; **29**: 15–21.
22. Robinson MD, McCarthy DJ, Smyth GK. edgeR: a Bioconductor package for differential expression analysis of digital gene expression data. *Bioinformatics* 2010; **26**: 139–140.
23. Ritchie ME, Phipson B, Wu D, *et al*. Limma powers differential expression analyses for RNA-sequencing and microarray studies. *Nucleic Acids Res* 2015; **43**: e47.
24. Su S, Law CW, Ah-Cann C, *et al*. Glimma: interactive graphics for gene expression analysis. *Bioinformatics* 2017; **33**: 2050–2052.
25. Bendall ML, de Mulder M, Iniguez LP, *et al*. Telescope: characterization of the retrotranscriptome by accurate estimation of transposable element expression. *PLoS Comput Biol* 2019; **15**: e1006453.
26. Taka JRH, Sun Y, Goldstone DC. Mapping the interaction between Trim28 and the KRAB domain at the center of Trim28 silencing of endogenous retroviruses. *Protein Sci* 2022; **31**: e4436.
27. Stoll GA, Pandiloski N, Douse CH, *et al*. Structure and functional mapping of the KRAB-KAP1 repressor complex. *EMBO J* 2022; **41**: e111179.
28. Stoll GA, Oda SI, Chong ZS, *et al*. Structure of KAP1 tripartite motif identifies molecular interfaces required for retroelement silencing. *Proc Natl Acad Sci U S A* 2019; **116**: 15042–15051.
29. Garcia-Barcena C, Osinalde N, Ramirez J, *et al*. How to inactivate human ubiquitin E3 ligases by mutation. *Front Cell Dev Biol* 2020; **8**: 39.
30. Zeng L, Yap KL, Ivanov AV, *et al*. Structural insights into human KAP1 PHD finger-bromodomain and its role in gene silencing. *Nat Struct Mol Biol* 2008; **15**: 626–633.

31. Hol JA, Diets IJ, de Krijger RR, *et al*. TRIM28 variants and Wilms' tumour predisposition. *J Pathol* 2021; **254:** 494–504.

32. Beckwith JB, Kiviat NB, Bonadio JF. Nephrogenic rests, nephroblastomatosis, and the pathogenesis of Wilms' tumor. *Pediatr Pathol* 1990; **10:** 1–36.

33. D'Hooghe E, Furtwangler R, Chowdhury T, *et al*. Stage I epithelial or stromal type Wilms tumors are low risk tumors: an analysis of patients treated on the SIOP-WT-2001 protocol in the UK-CCLG and GPOH studies (2001-2020). *Cancer* 2023; **129:** 1930–1938.

34. Gessler M, Graf N. Less may be more for stage I epithelial Wilms tumors. *Cancer* 2020; **126:** 2762–2764.

35. van den Heuvel-Eibrink MM, Hol JA, Pritchard-Jones K, *et al*. Position paper: rationale for the treatment of Wilms tumour in the UMBRELLA SIOP-RTSG 2016 protocol. *Nat Rev Urol* 2017; **14:** 743–752.

SUPPLEMENTARY MATERIAL ONLINE

Table S1. Primer sequences used

Table S2. Detailed molecular and clinical information of WT cases analyzed

Table S3. Differentially expressed genes between TRIM28 mutant versus wildtype tumors

---